Title

Crystal structure of Mdm12 and combinatorial reconstitution of Mdm12/Mmm1 ERMES complexes for structural studies.

Journal

Biochemical and biophysical research communications, 488(1)

ISSN

0006-291X

Authors

AhYoung, Andrew P
Lu, Brian
Cascio, Duilio
et al.

Publication Date

2017-06-01

DOI

10.1016/j.bbrc.2017.05.021

Peer reviewed

Biochemical and Biophysical Research Communications 488 (2017) 129–135

Contents lists available at ScienceDirect

Biochemical and Biophysical Research Communications

journal homepage: www.elsevier.com/locate/ybbrc

Crystal structure of Mdm12 and combinatorial reconstitution of Mdm12/Mmm1 ERMES complexes for structural studies

Andrew P. AhYoung [a, 1, 2], Brian Lu [a, 2], Duilio Cascio [b], Pascal F. Egea [a, b, *]

[a] Department of Biological Chemistry, David Geffen School of Medicine, UCLA, Los Angeles, USA
[b] Molecular Biology Institute, UCLA, Los Angeles, CA, USA

ARTICLE INFO

Article history:
Received 25 April 2017
Accepted 3 May 2017
Available online 4 May 2017

Keywords:
ERMES
Membrane contact sites
Mdm12/Mmm1 complex reconstitution
SMP domain
Crystal structure
SAXS

ABSTRACT

Membrane contact sites between organelles serve as molecular hubs for the exchange of metabolites and signals. In yeast, the Endoplasmic Reticulum – Mitochondrion Encounter Structure (ERMES) tethers these two organelles likely to facilitate the non-vesicular exchange of essential phospholipids. Present in Fungi and Amoebas but not in Metazoans, ERMES is composed of five distinct subunits; among those, Mdm12, Mmm1 and Mdm34 each contain an SMP domain functioning as a lipid transfer module. We previously showed that the SMP domains of Mdm12 and Mmm1 form a hetero-tetramer. Here we describe our strategy to diversify the number of Mdm12/Mmm1 complexes suited for structural studies. We use sequence analysis of orthologues combined to protein engineering of disordered regions to guide the design of protein constructs and expand the repertoire of Mdm12/Mmm1 complexes more likely to crystallize. Using this combinatorial approach we report crystals of Mdm12/Mmm1 ERMES complexes currently diffracting to 4.5 Å resolution and a new structure of Mdm12 solved at 4.1 Å resolution. Our structure reveals a monomeric form of Mdm12 with a conformationally dynamic N-terminal β-strand; it differs from a previously reported homodimeric structure where the N-terminal β strands where swapped to promote dimerization. Based on our electron microscopy data, we propose a refined pseudo-atomic model of the Mdm12/Mmm1 complex that agrees with our crystallographic and small-angle X-ray scattering (SAXS) solution data.

1. Introduction

Eukaryotic cells are characterized by their exquisite compartmentalization with a multitude of organelles each fulfilling specific functions essential to cellular life. Membrane contact sites (MCSs), regions where two organelles come in close proximity to one another, act as molecular hubs for the exchange of small molecules (*e.g.* lipids) and signals (*e.g.* calcium ions) [1,2]. Lipid exchange between organelles is important for the establishment of organelle identity and proper function. While the endoplasmic reticulum (ER) is the main site for phospholipid synthesis, other organelles such as the mitochondrion rely on inter-organelle lipid exchange processes for their biogenesis. Mitochondria attached membranes (MAMs) in particular have been involved in the exchange and transfer of phospholipids between organelles [3,4]. In yeast, the endoplasmic reticulum –mitochondrion encounter structure (ERMES) is one of the well-characterized inter-organelle tethering complexes [5]. Still in yeast, other tethers have been since discovered such as the mitochondrion-vacuole tether vCLAMP [6,7] and the conserved ER membrane protein complex EMC [8], another ER-mitochondrion tether.

The ERMES is composed of five subunits: The cytosolic protein Mdm12, the ER-anchored Mmm1 subunit and the three outer-mitochondrial membrane proteins Mdm34, Mdm10 and Gem1 [9,10]. Mdm12, Mmm1 and Mdm34 all contain a synaptotagmin-like mitochondrial lipid-binding domain (SMP) (Fig. 1A and B); SMP domains are exclusively found at MCSs between different organelles such as ER-Mitochondrion, ER-Plasma Membrane and Nucleus-Vacuole junctions [11]. The crystal structure of the extended synaptotagmin-2 (E-SYT2) [12], involved in ER to plasma membrane contact sites [13], revealed that the SMP domain belongs to the TULIP (for TUbular LIPid-binding) protein superfamily

* Corresponding author. UCLA David Geffen School of Medicine, Department of Biological Chemistry, Boyer Hall room 356, 611 Charles E. Young Drive East, CA 90095, Los Angeles, CA, USA.
E-mail address: pegea@mednet.ucla.edu (P.F. Egea).
[1] Present address: Department of Early Discovery Biochemistry, Genentech Inc., South San Francisco, California, USA.
[2] APAY and BL equally contributed to this work.

http://dx.doi.org/10.1016/j.bbrc.2017.05.021
0006-291X/

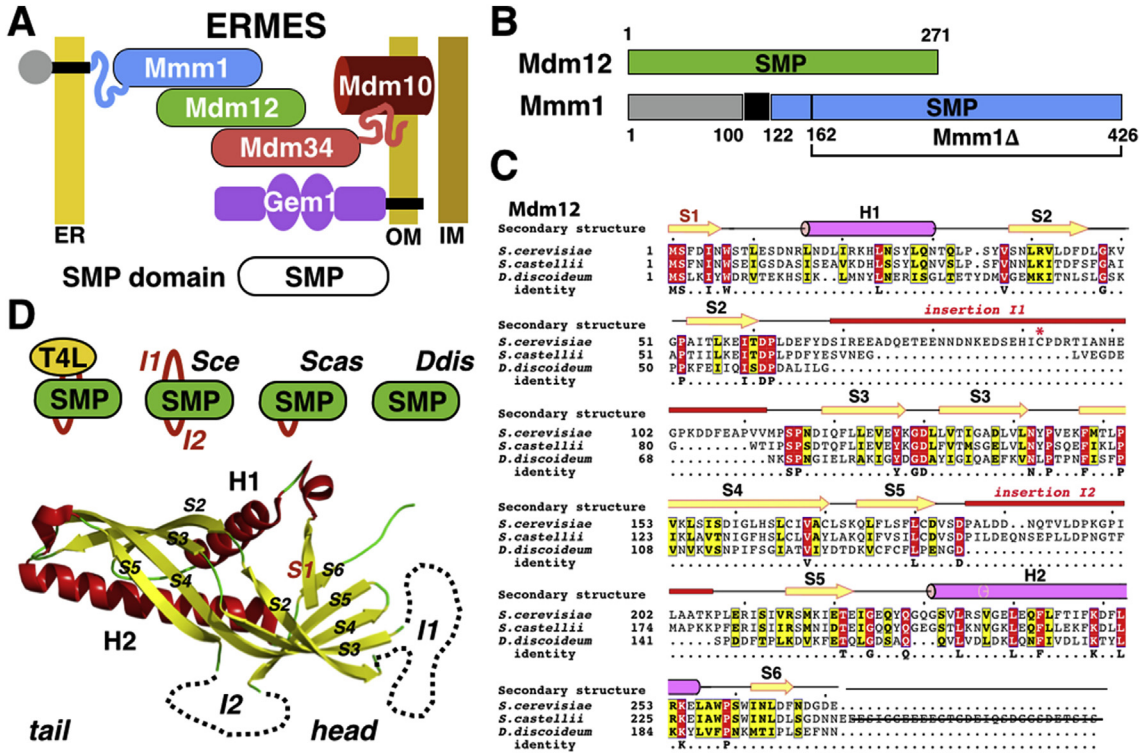

Fig. 1. ERMES and the SMP domain. **(A)** Schematic of the yeast ERMES bridging the endoplasmic reticulum (ER) and mitochondria (Outer and Inner) membranes. **(B)** Domain organization of yeast Mdm12 and Mmm1. Mdm12 consists of an SMP domain while Mmm1 contains a luminal domain (grey), one transmembrane anchor and a single cytoplasmic SMP domain (blue). **(C)** Protein sequence alignments of Mdm12 in *Saccharomyces cerevisiae*, *Saccharomyces castellii* and *Dictyostelium discoideum*. Non-conserved insertions (I1 and I2) are highlighted. Secondary structure elements are labeled. **(D)** Two variable insertions in the SMP fold of Mdm12: I1 (absent in *Scas* and *Ddis*) and I2 (absent in *Ddis*). The T4L insert replaces the longest insertion I1. (For interpretation of the references to colour in this figure legend, the reader is referred to the web version of this article.)

of lipid transfer proteins [14–16]. Biophysical studies using proteoliposomes also demonstrated that the SMP domain present in E-SYTs is required for the exchange of glycerophospholipids [17]. Last, a study using a novel *in vitro* assay system with isolated yeast membrane fractions suggested a phospholipid transfer function for ERMES [18]. We have shown that the SMP domains of Mdm12 and Mmm1 bind glycerophospholipids and assemble into a hetero-tetrameric complex. Our 17 Å resolution negative staining electron microscopy (NS-EM) structure revealed a distinctive architecture where two monomers of Mdm12 bind separately to a central ER-anchored Mmm1 homodimer [19]. These studies suggest that at MAMs, the SMP domains of ERMES directly mediate lipid transfer between the two organelles.

Our structural understanding of ERMES remains limited; we thus crystallized Mdm12 and the Mdm12/Mmm1 complex previously characterized in *Saccharomyces cerevisiae* (*Sce*). To grow suitable crystals we describe here the purification, characterization and reconstitution of several Mdm12 proteins and Mdm12/Mmm1 complexes by expanding the repertoire of Mdm12 proteins available through the combined use of orthologues and protein engineering to reduce disorder. We obtained diffracting crystals of Mdm12 and Mdm12/Mmm1 complex and solved a 4.1 Å resolution crystal structure of *Sce*-Mdm12 revealing the monomeric nature of the SMP domain and the structural plasticity of its N-terminus.

2. Materials and methods

2.1. Protein expression and complex reconstitution

Saccharomyces castellii (Scas) Mdm12 (residues S2-E244) and *Dictyostelium discoideum (Ddis)* Mdm12 (residues S2-N202) proteins were expressed as His-MBP fusions using a pCDF vector. The sequence coding the 162 residues of T4 lysozyme (T4L) was inserted in the *Sce*-Mdm12 gene between positions S88 and S115 in the non-conserved insertion I1 (Fig. 1C and D). The chimeric protein was expressed using a pJexpress411 plasmid (*DNA2.0 Inc.*) (Supplementary Fig. S1). All proteins were expressed and purified following protocols described in AhYoung et *al.* [19]. Complexes and proteins were purified by one final size exclusion chromatography (SEC) step on a Superdex S200 HR10/30 analytical SEC column (*GE Healthcare*) equilibrated in 200 mM Nacl, 20 mM Tris-HCl pH = 8.0, 2% glycerol, 0.1 mM TCEP and 0.1 mM PMSF (Fig. 2).

2.2. Mdm12 and Mmd12/Mmm1Δ complex crystallization

Crystallization screenings were performed by vapor diffusion at 4 °C in hanging drops using protein solutions concentrated at 15 mg/ml. Protein-to-reservoir ratios of 2-to-1, 1-to-1 and 1-to-2 were tested. Crystals of *Sce*-Mdm12 grew in 15–25% PEG 3,350, 400 mM ammonium phosphate and 3.5 mM Mega-10 (*Anatrace*); they diffracted to 4.1 Å resolution and belong to rhombohedral space group $P3_221$ with unit cell parameters a = b = 116.0 Å and c = 161.7 Å with two molecules in the asymmetric unit and 78% solvent. Crystals of complex diffracted to 4.5 Å resolution and belong to one of the tetragonal space groups in the P4/mmm Laue group with unit cell parameters a = b = 167 Å and c = 89.2 Å with 1 molecule of complex in the asymmetric unit and 54% solvent.

2.3. Diffraction data collection, structure determination, and refinement

Diffraction data were collected at the Advanced Photon Source

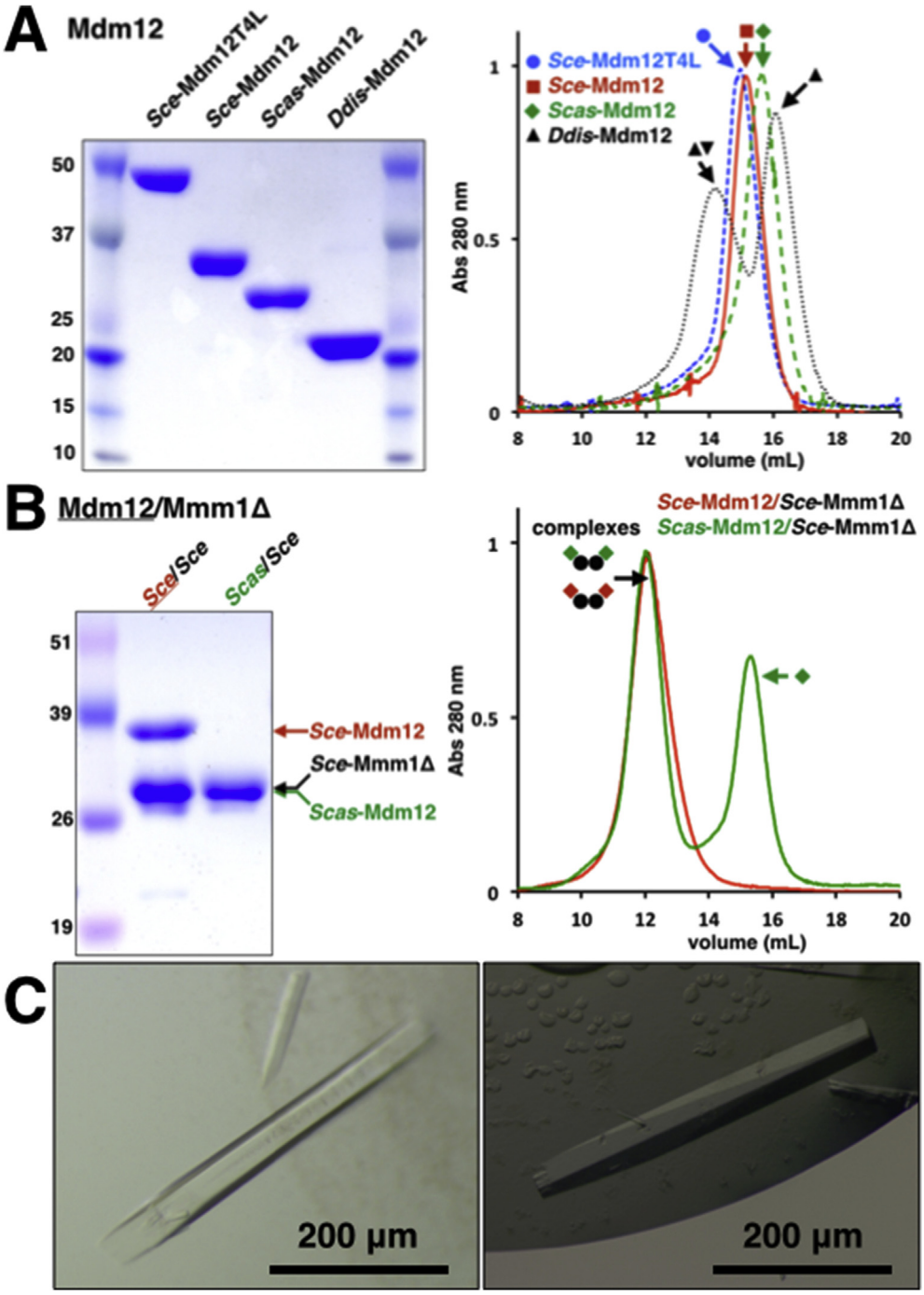

Fig. 2. Characterization of proteins and complexes by SDS-PAGE and SEC. **(A)** Mdm12 proteins. *Sce*, *Scas* and *Ddis* together with the Sce-Mdm12T4L internal fusion protein. The two *Ddis*-Mdm12 peaks correspond to a dimer/monomer mixture, all other proteins are monomeric. **(B)** Mdm12/Mmm1Δ heterotetrameric complexes. *Scas*-Mdm12 and *Sce*-Mmm1Δ have identical molecular weight and cannot be resolved on this gel. For *Scas*-Mdm12/Sce-Mmm1Δ complex, excess of free monomeric *Scas*-Mdm12 is separated from the complex. **(C)** Crystals of Mdm12/Mmm1Δ complexes.

in the Argonne National Laboratory and at the Advanced Light Source in the Lawrence Berkeley National Laboratory. Crystals were cryoprotected in mother liquor supplemented with 20–25% glycerol. Data were processed in *XDS* [20]. The structure of Mdm12 was solved by molecular replacement with *Phaser* [21] using the *Sce*-Mmd12 crystal structures described by Jeong et al. [22] (PDB accession codes 5GYD and 5GYK) as search probes. To minimize model bias, the search model consisted in the monomer where the 14 first residues, corresponding to the swapped N-terminal β-strand S1 and the connecting loop preceding helix H1 were removed; two copies of *Sce*-Mdm12 were located in the asymmetric unit. Inspection of the initial unbiased *Fo-Fc* map revealed that only one N-terminal β-strand S1, assigned to monomer A, could be located (Supplementary Fig. S2); the corresponding β-strand in monomer B cannot be located, likely disordered and flipped out towards the solvent. Given the low resolution of our diffraction data, we applied a negative thermal factor of −129 $Å^2$ estimated using the UCLA-DOE diffraction anisotropy server at

services.mbi.ucla.edu/anisoscale [23], to sharpen the experimental electron density maps [24,25]. B-sharpened electron density maps and data were exclusively used to guide model building but *not* used to refine the structure. We previously used a similar approach to refine a membrane protein structure [26]. In this case, original phases are based on a molecular replacement solution using an identical structure solved at a higher resolution (3.1 Å) and in a different space group. To avoid over-fitting, three refinement cycles were done, one in *Phenix* [27], and two in *Buster* [28]. Model building was done in *COOT* [29]. The final model is refined to R_{free} and R_{cryst} values of 26.3% and 24.8%, respectively, with acceptable stereochemistry and electron density maps (Supplementary Figs. S4 and S5). Crystallographic statistics are detailed in Supplementary Table 1.

2.4. Small-angle X-ray solution scattering

SAXS data were collected at the Advanced Light Source at the Lawrence Berkeley National Laboratory. Experimental conditions were as previously described [30,31]. Scattering curves for the complex model were calculated using *CRYSOL* [32] and pair distance distributions -*P(r)* - derived by Fourier inversion using *GNOM* [33] to estimate D_{max}, the longest distance occurring in the particle, and R_G, its radius of gyration.

3. Results and discussion

3.1. Identification of Mdm12 orthologues with fewer and/or shorter insertions

Bioinformatic analyses have identified ERMES in lineages outside Fungi [34]. The TULIP/SMP fold consists into a highly twisted β-sheet sandwiched between two α-helices; the resulting elongated barrel-shaped cylindrical structure harbors a lateral opening and a central hydrophobic cavity where phospholipids can bind. Sequence analysis of diverse Mdm12 protein sequences (Fig. 1C) and homology modeling reveal the presence of two non-conserved insertions I1 and I2 (Fig. 1D) located at the so-called 'head' region of the domain. The presence of long and/or disordered regions is a poor predictor of crystallization. Following this rationale, we sought to identify orthologues of *Sce*-Mdm12 with shorter insertions or no insertions. We identified two other Mdm12 proteins in *Saccharomyces castellii* and *Dictyostelium discoideum*. While *Sce*-Mdm12 harbors the two insertions, Mdm12 from the closely related yeast *Scas* only contains insertion I2 while its orthologue in the evolutionarily distant amoeba *Ddis* does not contain any of those insertions; *Ddis*-Mdm12 thus appears to represent a minimalistic version of the TULIP/SMP domain in the ERMES component Mdm12. To further expand our repertoire of constructs and improve the odds to grow diffracting crystals, we also applied an internal fusion protein engineering strategy [35] by replacing part of insertion I1 of *Sce*-Mdm12 with T4L.

3.2. Purification of Mdm12 orthologues and combinatorial reconstitution of Mdm12/Mmm1Δ complexes

While *Sce*-Mdm12 robustly expressed by itself in *E. coli* [19], it was necessary to express its orthologues from *Scas* and *Ddis* as N-terminal MBP fusions. Based on previous analyses [19], the orthologue from *Scas* and the T4L internal fusion protein behave as exclusive monomers in solution while the orthologue from *Ddis* is a mixture of dimers and monomers. While *Sce*-Mdm12 expressed in *E. coli* yields a mixture of dimers and monomers (although the monomer is more prominent), the same protein purified from its native organism (yeast) is only observed under its monomeric form [19]. Furthermore, the *Sce*-Mdm12T4L internal fusion protein is exclusively monomeric in solution (Fig. 2A).

We were able to purify the heterologous complex formed between *Sce*-Mmm1Δ and the Mdm12 protein from *Scas* but not from *Ddis* (Fig. 2B). This is not that surprising since the two proteins from the two different species of *Saccharomyces* are 58% identical while the Mdm12 from the amoeba *Dictyostelium* only shares ~20% sequence identity with its orthologues in *Saccharomyces* (Fig. 1D). We were also unable to form a complex between the SMP domains of *Sce*-Mmm1Δ and *Sce*-Mdm12T4L; this indicates that the presence of a bulky protein domain replacing most of the first non-conserved insertion I1 (Fig. 1D) does prevent complex formation. The two new complexes characterized in this study are hetero-tetramers of equimolecular stoichiometry.

3.3. Crystallization trials

Despite extensive effort, crystallization trials on Mdm12 orthologues met limited success, yielding numerous crystallization conditions with large but overall poorly diffracting crystals in the case of *Sce*-Mdm12 and, surprisingly, no crystals for the shorter Mdm12 versions from *Scas* and *Ddis* although we predicted them to be more amenable to crystallization. Crystals of *Sce*-Mdm12T4L proved difficult to reproduce. We eventually grew crystals of *Sce*-Mdm12 diffracting to 4.1 Å resolution. *Sce*-Mdm12/*Sce*-Mmm1Δ and *Scas*-Mdm12/*Sce*-Mmm1Δ complexes yielded also numerous crystals forms (Fig. 2C) that we are currently optimizing for diffraction data collection; the current diffraction limit is about 4.5 Å (Supplementary Table 1).

3.4. The crystal structure of a monomeric form of yeast Mdm12 reveals a dynamic N-terminus

We describe a new crystal structure of *Sce*-Mdm12 solved by molecular replacement at 4.1 Å resolution using the crystal structures of *Sce*-Mdm12 recently published by Jeong et al. [22] as search models. Our structure corresponds to a different crystal form (*i.e.* rhombohedral *vs* orthorhombic) and crystallization condition. The high solvent (~78%) content and weak crystal packing explain the poor diffraction and high estimated Wilson B thermal factor (~143 $Å^2$). We do not observe bound phospholipids. Our structure thus corresponds to an *apo* state of Mdm12 in contrast with Jeong et al. [22]; the use of detergent MEGA-10 for crystallization might explain the *apo*-state.

The presence of a N-terminal β-strand (S1) is a distinctive feature of the SMP fold of Mdm12 (and by homology also Mdm34) in opposition with the SMP domain of Mmm1 that is predicted to be structurally more similar to the SMP of E-SYT2 [19,22]. Differences between the Mdm12 and the E-SYT2 SMP structures were significant enough to prevent solving the structure by molecular replacement using the E-SYT2 crystal structure or homology models based on all available structures from other TULIP proteins (Supplemental Fig. S3).

In our case, Mdm12 crystallized in a rhombohedral space group in contrast with the orthorhombic crystal forms previously reported. These different crystalline form and packing reveal the dynamic behavior of the TULIP/SMP domain in Mdm12. Although two molecules of Mdm12 are present in the asymmetric unit, we do not observe a swapped dimer where the first N-terminal β strands S1 are exchanged to complete the 'head-to-head' dimerization interface (Fig. 3A) reported by Jeong et al. [22]. Furthermore, within the asymmetric unit, the two monomers differ in the conformation adopted by their N-terminal β-strands S1. In monomer A, β-strand S1 is well resolved in the electron density map and hydrogen bonds with β-strand S2 of the *same* monomer; thus it adopts a non-

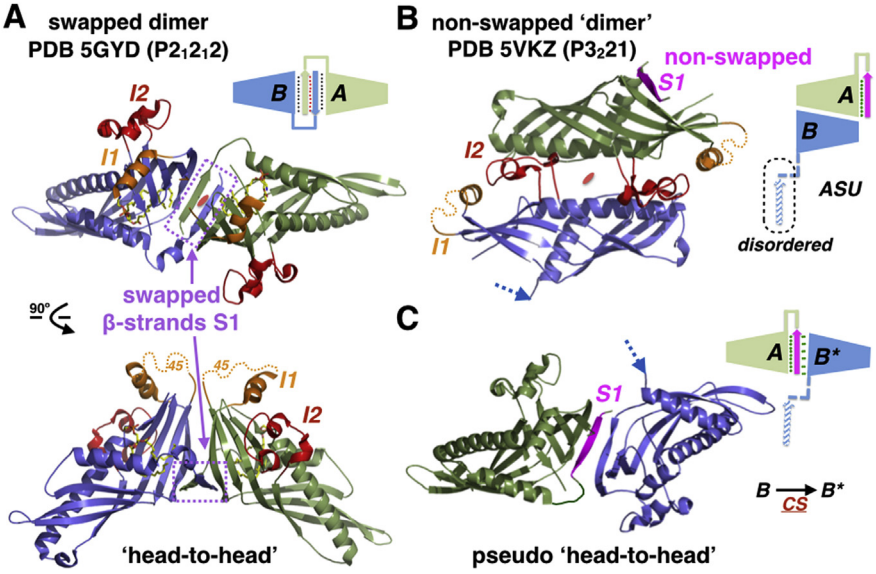

Fig. 3. A new crystal structure of *Sce*-Mdm12. **(A)** Swapped 'head-to-head' dimer of *Sce*-Mdm12 observed in the 3.1 Å resolution orthorhombic structure from Jeong et al. [22]. **(B)** Non-swapped dimer of *Sce*-Mdm12 observed in our 4.1 Å resolution rhombohedral structure. Two monomers (A and B) are observed in the asymmetric unit. In monomer A, the N-terminal β-strand S1 (magenta) is resolved in the electron density but does not swap. The N-terminal β-strand S1 of monomer B has flipped into a solvent-exposed conformation and cannot be resolved in the electron density maps. Insertions I1 and I2 are colored in gold and red, respectively. **(C)** A crystallographic symmetry-related copy of monomer B (note B*), forms a pseudo 'head-to-head' dimer where only one β-strand S1 (from monomer A) sits at the interface between the two SMP/TULIP domains. CS indicates that B and B* are related by a $P3_221$crystallographic symmetry operator. (For interpretation of the references to colour in this figure legend, the reader is referred to the web version of this article.)

swapped conformation. On the other hand, the N-terminal β-strand S1 of monomer B cannot be traced and is likely to be flipped towards the solvent; it is clearly *not* engaged in the same intermolecular interactions observed in monomer A (Fig. 3B). Despite the modest resolution of our data, this structural difference is unambiguous as demonstrated by the maximum likelihood weighted m*Fo*-D*Fc* Fourier difference map obtained after molecular replacement using a search model consisting of the monomer of Mdm12 where the first 14 residues were omitted (Supplemental Fig. S2). The non-crystallographic dimer observed in our crystal form corresponds to an 'anti-parallel' arrangement along the long α-helix H2 that is part of the TULIP/SMP fold; this large crystal contact interface is also observed in the Mdm12 structures recently published [22] although it does not involve residues conserved among all Mdm12 sequences.

The most peculiar aspect of the crystal packing in our rhombohedral crystal form resides in the fact that two Mdm12 monomers (*i.e.* monomer A and a crystallographic-symmetry related copy of monomer B, labeled B*) form a pseudo-dimer where the two molecules associate in a 'head-to-head' arrangement (Fig. 3C); although the two resulting 'head-to-head' Mdm12 dimers might look identical, they are not (Supplementary Fig. S6). Thus, although there is no swapping *within the asymmetric unit* there is partial swapping *within the unit cell* as one β-strand S1 from one SMP displaces and replaces the β-strand S1 of another SMP while still interacting with its own SMP. Within the non-swapped monomer A of our structure, β-strands S1 and S2 adopt an anti-parallel arrangement, this is the opposite of what is observed in the swapped dimers from Jeong et al. [22] where the swapped β-strands S1 and S2 run parallel to each other; however, in our asymmetric pseudo-dimer interface (A/B*) the two β-strands, S1 from monomer A and S2 from monomer B*, associate in a parallel arrangement.

This unusual case of 'broken' symmetry underlines two important functional aspects of the SMP domain of Mdm12 and also potentially of Mdm34 that shares a similar N-terminal sequence: First, the N-terminal β-strand of the SMP domain of Mdm12 is dynamic; second, the putative 'head-to-head' dimerization interface of Mdm12 appears to be somehow promiscuous. The basis for that promiscuity is rooted in the type of interactions that mediates association between the two SMP domains: Mdm12 SMP 'dimerization' is essentially driven by strand S1-to-strand S1 interactions through backbone-to-backbone hydrogen bonds (Supplementary Fig. S7). Within our non-swapped monomer A, N-terminal β-strand S1 completes the canonical TULIP/SMP anti-parallel β-barrel through its association with β-strand S2. The anti-parallel arrangement of β-strands into β-sheets is thermodynamically favored because it allows the inter-strand hydrogen bonds between carbonyls and amines to be planar, which is their preferred orientation; this arrangement results in a strongest inter-strand stability.

3.5. Solution conformation and improved pseudo-model of the Mdm12/Mmm1 heterotetramer of SMP domains

We published a 17 Å resolution NS-EM structure of the *Sce*-Mdm12/Mmm1Δ hetero-tetramer [19] where we established the number of Mmm1 and Mdm12 subunits present, together with their relative positions, within the elongated crescent-shaped complex (Fig. 4A). Our predictions supported a model where two Mmm1 SMP domains associate to form a homodimer similar to the 'head-to-head' E-SYT2 homodimer of SMP domains [12] (Fig. 4B). EM electron density maps display a distinct mass of density near the putative Mmm1-to-Mdm12 interface (Fig. 4B). The best fit between EM density and crystal structures can only be achieved through a 'tail-to-head' association between the 'tail' of Mmm1 and the 'head' of Mdm12 (Fig. 4). A last argument in favor of this model resides in the observation that the *Sce*-Mdm12T4L protein cannot form a complex; given the position of the fused T4L near the 'head' region (Fig. 1D), the resulting steric hindrance could prevent association with Mmm1.

We characterized the solution conformation of the *Sce*-Mdm12/Mmm1Δ complex using SAXS [36] by comparing its experimental pair distance distribution with the one calculated using our pseudo-model based on NS-EM and crystallographic data. The

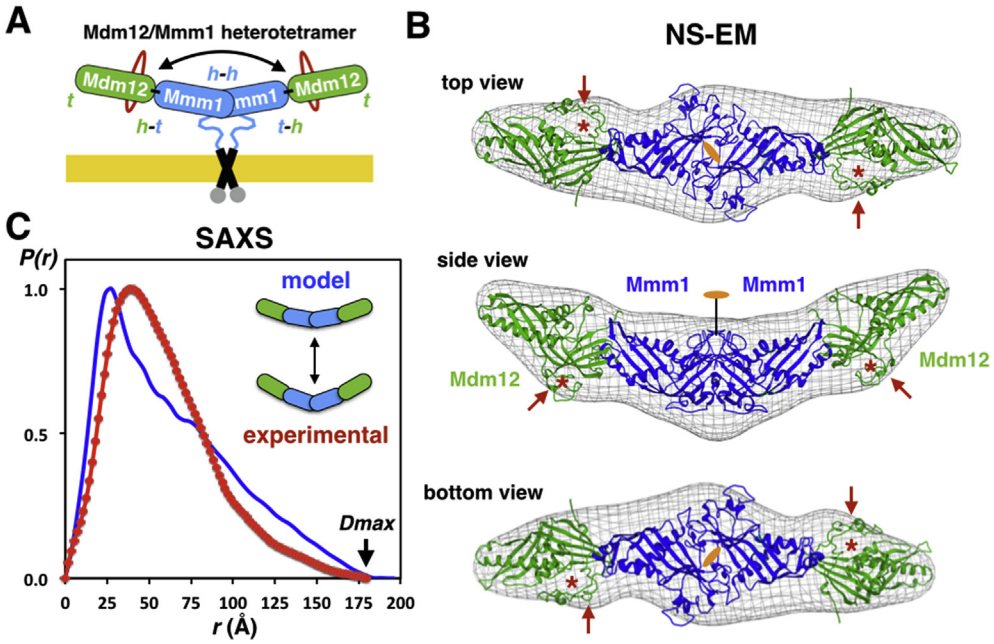

Fig. 4. Pseudo-atomic model of the Sce-Mdm12/Mmm1Δ hetero-tetramer and solution scattering analysis of its average conformation (A). Schematic model of the Mdm12/Mmm1 complex. Insertions in Mdm12 are depicted in red; h and t correspond to the 'head' and 'tail' regions of each of the four SMP domains, respectively. The 'head-to-head' dimer of Mmm1 SMP domains is anchored to the ER membrane. The double arrow highlights the curvature/bent of the complex. **(B)** Fitting of our Mdm12/Mmm1Δ model using the crystal structure of *Sce*-Mdm12 in the EM density maps [19]. Red arrows and asterisks indicate the two insertions located next to the 'head' in yeast Mdm12. Three views are shown. **(C)** SAXS analysis of the *Sce*-Mdm12/Mmm1Δ complex. Comparison of the pair distance distributions determined from experimental scattering data (red) or calculated using our NS-EM/crystallographic mode (blue). (For interpretation of the references to colour in this figure legend, the reader is referred to the web version of this article.)

experimental curve is characteristic of a rod-like elongated structure [37]; the longest distance D_{max} of ~185 Å is close to the one inferred from the model and can only result from four SMP domains aligning along their longest axis. Variation in the curvature/bend of the complex could explain the discrepancy between experimental and calculated R_G and D_{max} values (Fig. 4C and Supplementary Table S2).

3.6. Interactions between SMP domains and assembly of ERMES

Interactions between the SMP domains of Mdm12 and Mmm1 are strong. We previously showed that the three SMP domains of Mmm1, Mdm12, and Mdm34 form a weak ternary complex and that Mdm12 and Mdm34 are interacting directly [19] suggesting that Mdm12 acts as a bridging subunit between the ER-bound Mmm1 and the mitochondria-bound subunits Mdm34 and Mdm10. Jeong et al. [22] showed evidence for a weak interaction between Mdm12 and a fragment of Mdm34 corresponding to the first residues of its SMP domain and observed that the N-termini of Mdm12 and Mdm34 share common sequence and secondary structure features. Thus, the conformational dynamics and plasticity of the N-terminus of the SMP domain of Mdm12 revealed by two distinct crystal structures might also apply to Mdm34. Although both monomeric and dimeric forms of Mdm12 have been observed in solution and their crystal structures determined, their biological significance needs to be further investigated. Our model predicts that the N-terminus of Mdm12 is engaged at the Mdm12/Mmm1 interface, thus formation of "our" complex implies dissociation of a swapped Mdm12 homodimer. The structure of the Mdm12/Mmm1 complex will provide valuable insights into the molecular mechanisms for the transfer of phospholipids by the SMP domains of ERMES at MAMs.

Accession number

Coordinates and structure factors have been deposited under the Protein Data Bank accession code: 5VKZ.

Acknowledgements

This work was supported by the UCLA Geffen School of Medicine, the Stein-Oppenheimer Seed Grant Award and the Alexander and Renée Kolin Endowed Chair in Molecular Biology and Biophysics to P.F.E. A.P.A.Y. was supported by a Gates Millennium Fellowship and the UCLA Dissertation of the Year Fellowship. We thank the staffs from beamlines 24-ID (APS), 8.3.1 and 12.3.1 (ALS) for their assistance.

Appendix A. Supplementary data

Supplementary data related to this article can be found at http://dx.doi.org/10.1016/j.bbrc.2017.05.021.

Transparency document

Transparency document related to this article can be found online at http://dx.doi.org/10.1016/j.bbrc.2017.05.018.

References

[1] S. Lahiri, A. Toulmay, W.A. Prinz, Membrane contact sites, gateways for lipid homeostasis, Curr. Opin. Cell Biol. 33 (2015) 82–87.
[2] A. Gonzalez Montoro, C. Ungermann, StARTing to understand membrane contact sites, Trends Cell Biol. 25-9 (2015) 497–498.
[3] J.E. Vance, MAM (mitochondria-associated membranes) in mammalian cells: lipids and beyond, Biochim. Biophys. Acta 1841 (2014) 595–609.
[4] J.E. Vance, Phospholipid synthesis and transport in mammalian cells, Traffic 16 (2015) 1–18.

[5] B. Kornmann, E. Currie, S.R. Collins, M. Schuldiner, J. Nunnari, J.S. Weissman, P. Walter, An ER-mitochondria tethering complex revealed by a synthetic biology screen, Science 325 (2009) 477–481.
[6] Y. Elbaz-Alon, E. Rosenfeld-Gur, V. Shinder, A.H. Futerman, T. Geiger, M. Schuldiner, A dynamic interface between vacuoles and mitochondria in yeast, Dev. Cell 30 (2014) 95–102.
[7] C. Honscher, M. Mari, K. Auffarth, M. Bohnert, J. Griffith, W. Geerts, M. van der Laan, M. Cabrera, F. Reggiori, C. Ungermann, Cellular metabolism regulates contact sites between vacuoles and mitochondria, Dev. Cell 30 (2014) 86–94.
[8] S. Lahiri, J.T. Chao, S. Tavassoli, A.K. Wong, V. Choudhary, B.P. Young, C.J. Loewen, W.A. Prinz, A conserved endoplasmic reticulum membrane protein complex (EMC) facilitates phospholipid transfer from the ER to mitochondria, PLoS Biol. 12 (2014) e1001969.
[9] B. Kornmann, C. Osman, P. Walter, The conserved GTPase Gem1 regulates endoplasmic reticulum-mitochondria connections, Proc. Natl. Acad. Sci. U. S. A. 108 (2011) 14151–14156.
[10] D.A. Stroud, S. Oeljeklaus, S. Wiese, M. Bohnert, U. Lewandrowski, A. Sickmann, B. Guiard, M. van der Laan, B. Warscheid, N. Wiedemann, Composition and topology of the endoplasmic reticulum-mitochondria encounter structure, J. Mol. Biol. 413 (2011) 743–750.
[11] A. Toulmay, W.A. Prinz, A conserved membrane-binding domain targets proteins to organelle contact sites, J. Cell Sci. 125 (2012) 49–58.
[12] C.M. Schauder, X. Wu, Y. Saheki, P. Narayanaswamy, F. Torta, M.R. Wenk, P. De Camilli, K.M. Reinisch, Structure of a lipid-bound extended synaptotagmin indicates a role in lipid transfer, Nature 510 (2014) 552–555.
[13] R. Fernandez-Busnadiego, Y. Saheki, P. De Camilli, Three-dimensional architecture of extended synaptotagmin-mediated endoplasmic reticulum-plasma membrane contact sites, Proc. Natl. Acad. Sci. U. S. A. 112 (2015) E2004–E2013.
[14] K.O. Kopec, V. Alva, A.N. Lupas, Homology of SMP domains to the TULIP superfamily of lipid-binding proteins provides a structural basis for lipid exchange between ER and mitochondria, Bioinformatics 26 (2010) 1927–1931.
[15] K.M. Reinisch, P. De Camilli, SMP-domain proteins at membrane contact sites: structure and function, Biochim. Biophys. Acta 18-5 (2015) 504–515.
[16] V. Alva, A.N. Lupas, The TULIP superfamily of eukaryotic lipid-binding proteins as a mediator of lipid sensing and transport, Biochim. Biophys. Acta 1861 (2016) 913–923.
[17] Y. Saheki, X. Bian, C.M. Schauder, Y. Sawaki, M.A. Surma, C. Klose, F. Pincet, K.M. Reinisch, P. De Camilli, Control of plasma membrane lipid homeostasis by the extended synaptotagmins, Nat. Cell Biol. 18 (2016) 504–515.
[18] R. Kojima, T. Endo, Y. Tamura, A phospholipid transfer function of ER-mitochondria encounter structure revealed in vitro, Sci. Rep. 6 (2016) 30777.
[19] A.P. AhYoung, J. Jiang, J. Zhang, X. Khoi Dang, J.A. Loo, Z.H. Zhou, P.F. Egea, Conserved SMP domains of the ERMES complex bind phospholipids and mediate tether assembly, Proc. Natl. Acad. Sci. U. S. A. 112 (2015) E3179–E3188.
[20] W. Kabsch, Xds, Acta Crystallogr. D. Biol. Crystallogr. 66 (2010) 125–132.
[21] A.J. McCoy, R.W. Grosse-Kunstleve, P.D. Adams, M.D. Winn, L.C. Storoni, R.J. Read, Phaser crystallographic software, J. Appl. Crystallogr. 40 (2007) 658–674.
[22] H. Jeong, J. Park, C. Lee, Crystal structure of Mdm12 reveals the architecture and dynamic organization of the ERMES complex, EMBO Rep. 17 (2016) 1857–1871.
[23] M. Strong, M.R. Sawaya, S. Wang, M. Phillips, D. Cascio, D. Eisenberg, Toward the structural genomics of complexes: crystal structure of a PE/PPE protein complex from Mycobacterium tuberculosis, Proc. Natl. Acad. Sci. U. S. A. 103 (2006) 8060–8065.
[24] B. DeLaBarre, A.T. Brunger, Considerations for the refinement of low-resolution crystal structures, Acta Crystallogr. Sect. D-Biol. Crystallogr. 62 (2006) 923–932.
[25] A.T. Brunger, B. DeLaBarre, J.M. Davies, W.I. Weis, X-ray structure determination at low resolution, Acta Crystallogr. Sect. D-Biol. Crystallogr. 65 (2009) 128–133.
[26] P.F. Egea, R.M. Stroud, Lateral opening of a translocon upon entry of protein suggests the mechanism of insertion into membranes, Proc. Natl. Acad. Sci. U. S. A. 107 (2010) 17182–17187.
[27] P.D. Adams, P.V. Afonine, G. Bunkoczi, V.B. Chen, N. Echols, J.J. Headd, L.W. Hung, S. Jain, G.J. Kapral, R.W. Grosse Kunstleve, A.J. McCoy, N.W. Moriarty, R.D. Oeffner, R.J. Read, D.C. Richardson, J.S. Richardson, T.C. Terwilliger, P.H. Zwart, The Phenix software for automated determination of macromolecular structures, Methods 55 (2011) 94–106.
[28] E. Blanc, P. Roversi, C. Vonrhein, C. Flensburg, S.M. Lea, G. Bricogne, Refinement of severely incomplete structures with maximum likelihood in BUSTER-TNT, Acta Crystallogr. Sect. D-Biol. Crystallogr. 60 (2004) 2210–2221.
[29] P. Emsley, K. Cowtan, Coot: model-building tools for molecular graphics, Acta Crystallogr. D. Biol. Crystallogr. 60 (2004) 2126–2132.
[30] M. Peng, D. Cascio, P.F. Egea, Crystal structure and solution characterization of the thioredoxin-2 from Plasmodium falciparum, a constituent of an essential parasitic protein export complex, Biochem. Biophys. Res. Commun. 456 (2015) 403–409.
[31] A.P. AhYoung, A. Koehl, D. Cascio, P.F. Egea, Structural mapping of the ClpB ATPases of Plasmodium falciparum: targeting protein folding and secretion for antimalarial drug design, Protein Sci. 24 (2015) 1508–1520.
[32] D.I. Svergun, C. Barberato, M.H. Koch, CRYSOL: a program to evaluate X-ray solution scattering of biological macromolecules from atomic coordinates, J. Appl. Crystallogr. 28 (1995) 768–773.
[33] D.I. Svergun, Determination of the regularization parameter in indirect transform methods using perceptual criteria, J. Appl. Crystallogr. 25 (1992) 495–503.
[34] J.G. Wideman, R.M.R. Gawryluk, M.W. Gray, J.B. Dacks, The ancient and widespread nature of the ER-mitochondria encounter structure, Mol. Biol. Evol. 30 (2013) 2044–2049.
[35] G.G. Prive, G.E. Verner, C. Weitzman, K.H. Zen, D. Eisenberg, H.R. Kaback, Fusion proteins as tools for crystallization: the lactose permease from Escherichia coli, Acta Crystallogr. D. Biol. Crystallogr. 50 (1994) 375–379.
[36] C.E. Blanchet, D.I. Svergun, Small-angle X-ray scattering on biological macromolecules and nanocomposites in solution, Annu. Rev. Phys. Chem. 64 (2013) 37–54.
[37] E. Ortega, J.A. Manso, R.M. Buey, A.M. Carballido, A. Carabias, A. Sonnenberg, J.M. de Pereda, The structure of the plakin domain of plectin reveals an extended rod-like shape, J. Biol. Chem. 291 (2016) 18643–18662.

Crystal structure of Mdm12 and combinatorial reconstitution of Mdm12/Mmm1 ERMES complexes for structural studies
A.P. AhYoung *et al.*
Biochemical and Biophysical Research Communications **488**, 129-135 *(2017)* **http://dx.doi.org/10.1016/j.bbrc.2017.05.021**

Appendix A. Supplementary data

Table S1. Diffraction data collection and structure refinement statistics

Protein	***Sce*-Mdm12 PDB ID 5VKZ**	**Mdm12/ Mmm1Δ**
Data set	**APS 042311 24-ID-C**	**ALS 101716 831**
Data collection statistics		
Wavelength	0.97918 Å	0.97918 Å
Resolution (last shell)	85.3-4.1 Å (4.21-4.10 Å)	20.13-4.50 Å (4.62-4.50 Å)
Unique reflections	10,272 (744)	7,867 (564)
Completeness	99.5 % (99.7 %)	98.3 % (99.8 %)
I/σ(I)	9.4 (2.0)	16.6 (1.6)
redundancy	7.4 (7.5)	3.9 (3.8)
R_{sym}	10.6 % (98.1 %)	3.1 % (93.5 %)
R_{meas} [a]	11.5 % (105.4 %)	3.6 % (108.9 %)
CC(1/2) [b]	99.8 % (95.8 %)	100.0 % (65.5 %)
Space group	$P3_221$	4/mmm (Laue class)
Unit cell dimensions	a=b=116.0 Å and c=161.7 Å	a=b=167.0 Å c=89.2 Å
AU content	2 molecules (pseudo-dimer)	1 complex
Solvent content	78 %	54 %
Refinement statistics		
Resolution	85.3-4.1 Å (4.58-4.10 Å)	-
Reflections	10,248	-
work set / test set	9,229 / 1,019	-
R_{free} / R_{cryst}	26.3 % / 24.8 %	-
Map correlation *Fo-Fc* (free)	82.8 % (88.0 %)	-
ESD Luzzati plot	1.383 Å	-
B_{wilson}	143 $Å^2$	-
$B_{average}$	162 $Å^2$	-
rmsd bonds	0.01 Å	-
rmsd angles	1.32 °	-
Ramachandran analysis		
allowed regions	88.9%	-
generously allowed	9.2%	-
outliers	1.4%	-

r.m.s.d. is the root-mean square deviation from ideal geometry.
$R_{sym} = \sum_{hkl}\sum_i |I_{hkl,i}-\langle I_{hkl,i}\rangle|/\sum_{hkl}\sum_i |I_{hkl,i}|$ where $\langle I_{hkl,i}\rangle$ is the average intensity of the multiple hkl, i observations for symmetry-related reflections.
R_{meas} is the redundancy independent R-factor [1].
CC(1/2) percentage of correlation between intensities from random half-datasets [2].
$R_{cryst} = \sum|F_{obs}-F_{calc}|/\sum|F_{obs}|$. F_{obs} and F_{calc} are observed and calculated structure factors, R_{free} is calculated from a set of randomly chosen reflections (10%), and R_{cryst} is calculated over the remaining reflections.
Structure quality was assessed in *MolProbity* [3] and *Polygon* [4].

Table S2. Small angle X-ray scattering analysis of the Mdm12/Mmm1Δ complex

protein	oligomeric state	calculated values from structures [a]		experimental values determined by SAXS [b] *Fourier analysis*	
		R_G	D_{max}	R_G	D_{max}
Mdm12	**monomer**	**21.9 Å**	**72 Å**	**-**	**-**
	dimer	**30.7 Å**	**108 Å**	**-**	**-**
complex	**hetero-tetramer**	**55.3 Å**	**195 ± 5 Å**	**46.7 ± 0.3 Å**	**185 ± 5 Å**

[a] the sets of theoretical R_G and D_{max} values correspond to the monomeric X-ray structure described in this study (PDB 5VKZ), the previously published Mdm12 dimeric structures (PDBs 5GYD and 5GYK) [5] and our pseudo-atomic model based on our NS-EM data of the Mdm12/Mmm1Δ complex [6], as shown in Figures 4A and 4B.

[b] experimental values of R_G and D_{max} were determined for the Mdm12/Mmm1Δ complex purified and crystallized as described in this work. Concentration of sample analyzed by SAXS ranged from 0.75 to 3 mg/ml and 4.8 to 14 mg/ml for the Guinier (low *q* range) and *P(r)* (high *q* range) analyses, respectively.

Crystal structure of Mdm12 and combinatorial reconstitution of Mdm12/Mmm1 ERMES complexes for structural studies
A.P. AhYoung *et al.*
Biochemical and Biophysical Research Communications **488**, 129-135 *(2017)* **http://dx.doi.org/10.1016/j.bbrc.2017.05.021**

pRSF His-MBP-Sce Mmm1Δ 31,219 Da

MGHHHHHHHHKIEEGKLVIWINGDKGYNGLAEVGKKFEKDTGIKVTVEHPDKLEEKFPQVAATGDGPDIIFWAHDRFGGYAQSGLL
AEITPDKAFQDKLYPFTWDAVRYNGKLIAYPIAVEALSLIYNKDLLPNPPKTWEEIPALDKELKAKGKSALMFNLQEPYFTWPLIA
ADGGYAFKYENGKYDIKDVGVDNAGAKAGLTFLVDLIKNKHMNADTDYSIAEAAFNKGETAMTINGPWAWSNIDTSKVNYGVTVLP
TFKGQPSKPFVGVLSAGINAASPNKELAKEFLENYLLTDEGLEAVNKDKPLGAVALKSYEEELAKDPRIAATMENAQKGEIMPNIP
QMSAFWYAVRTAVINAASGRQTVDEALKDAQTNSSSPGLVPRGSGKQHYELNEEAENEHLQELALILEKTYYNVDVHPAESLDWFN
VLVAQIIQQFRSEAWHRDNILHSLNDFIGRKSPDLPEYLDTIKITELDTGDDFPIFSNCRIQYSPNSGNKKLEAKIDIDLNDHLTL
GVETKLLLNYPKPGIAALPINLVVSIVRFQACLTVSLTNAEEFASTSNGSSSENGMEGNSGYFLMFSFSPEYRMEFEIKSLIGSRS
KLENIPKIGSVIEYQIKKWFVERCVEPRFQFVRLPSMWPRSKNTREEKPTELLVPRGSHHHHHHHHHH*

pCDF *Sce* Mdm12-His (C92S point mutation) 31,178 Da

MSFDINWSTLESDNRLNDLIRKHLNSYLQNTQLPSYVSNLRVLDFDLGKVGPAITLKEITDPLDEFYDSIREEADQETEENNDNKE
DSEHISPDRTIANHEGPKDDFEAPVVMPSPNDIQFLLEVEYKGDLLVTIGADLVLNYPVEKFMTLPVKLSISDIGLHSLCIVACLS
KQLFLSFLCDVSDPALDDNQTVLDPKGPILAATKPLERISIVRSMKIETEIGEQYQGQGSVLRSVGELEQFLFTIFKDFLRKELAW
PSWINLDFNDGDELVPRGSHHHHHH*

pCDF His-MBP-*Scas* Mdm12 27,709 Da

MGHHHHHHHHKIEEGKLVIWINGDKGYNGLAEVGKKFEKDTGIKVTVEHPDKLEEKFPQVAATGDGPDIIFWAHDRFGGYAQSGLL
AEITPDKAFQDKLYPFTWDAVRYNGKLIAYPIAVEALSLIYNKDLLPNPPKTWEEIPALDKELKAKGKSALMFNLQEPYFTWPLIA
ADGGYAFKYENGKYDIKDVGVDNAGAKAGLTFLVDLIKNKHMNADTDYSIAEAAFNKGETAMTINGPWAWSNIDTSKVNYGVTVLP
TFKGQPSKPFVGVLSAGINAASPNKELAKEFLENYLLTDEGLEAVNKDKPLGAVALKSYEEELAKDPRIAATMENAQKGEIMPNIP
QMSAFWYAVRTAVINAASGRQTVDEALKDAQTNSSSPGLVPRGSFNINWSEIGSDASISEAVKDHLSSYLQNVSLPSFVNNLKITD
FSFGAIAPTIILKEITDPLPDFYESVNEGLVEGDEGWTIPSPSDTQFLIEVEYKGDLFVTMSGELVLNYPSQEFIKLPIKLAVTNI
GFHSLCLVAYLAKQIFVSILCDVSDPILDEQNSEPLLDPNGTFMAPKKPFERISIIRSMNIDTEIGQQYQGEGSTLKNVGKLEQFL
LEKFKDLLRKEIAWPSWINLDLSGDNNELVPRGSHHHHHH*

pCDF His-MBP-*Ddis* Mdm12 23,171 Da

MGHHHHHHHHKIEEGKLVIWINGDKGYNGLAEVGKKFEKDTGIKVTVEHPDKLEEKFPQVAATGDGPDIIFWAHDRFGGYAQSGLL
AEITPDKAFQDKLYPFTWDAVRYNGKLIAYPIAVEALSLIYNKDLLPNPPKTWEEIPALDKELKAKGKSALMFNLQEPYFTWPLIA
ADGGYAFKYENGKYDIKDVGVDNAGAKAGLTFLVDLIKNKHMNADTDYSIAEAAFNKGETAMTINGPWAWSNIDTSKVNYGVTVLP
TFKGQPSKPFVGVLSAGINAASPNKELAKEFLENYLLTDEGLEAVNKDKPLGAVALKSYEEELAKDPRIAATMENAQKGEIMPNIP
QMSAFWYAVRTAVINAASGRQTVDEALKDAQTNSSSPGLVPRGSLKIYWDRVTEKHSIKLMNYLNERISGLTETYDMVGEMKITNL
SLGSKPPKFEIIQISDPDALILGNKSPNGIELRAKIGYDGDAYIGIQAEFKVNLPTPNFISFPVNVKVSNPIFSGIATVIYDTDKV
SFSFLPENGDSPDDFTPLKDVKFETQLGDSAQQVLVDLDKLQNFIVDLIKTYLKKYLVFPNKMTIPLSEFNNLVPRGSHHHHHH*

pJexp *Sce* Mdm12T4L-His 46,878 Da

MSFDINWSTLESDNRLNDLIRKHLNSYLQNTQLPSYVSNLRVLDFDLGKVGPAITLKEITDPLDEFYDSIREEADQETEENNDNKE
DSGSSGNIFEMLRIDEGLRLKIYKDTEGYYTIGIGHLLTKSPSLNAAKSELDKAIGRNTNGVITKDEAEKLFNQDVDAAVRGILRN
AKLKPVYDSLDAVRRAALINMVFQMGETGVAGFTNSLRMLQQKRWDEAAVNLAKSRWYNQTPNRAKRVITTFRTGTWDAYAAGSPN
DIQFLLEVEYKGDLLVTIGADLVLNYPVEKFMTLPVKLSISDIGLHSLCIVACLSKQLFLSFLCDVSDPALDDNQTVLDPKGPILA
ATKPLERISIVRSMKIETEIGEQYQGQGSVLRSVGELEQFLFTIFKDFLRKELAWPSWINLDFNDGDELVPRGSHHHHHHHHH*

Histidine tag
Maltose Binding Protein
Proteolytic cleavage site for thrombin.
Mdm12 or Mmm1 protein. Underlined residues were replaced with the T4L protein insertion in the internal *Sce*-Mdm12T4L chimeric construct.
T4 Lysozyme

Fig. S1. Protein constructs used for the reconstitution of the different Mdm12 and Mdm12/ Mmm1Δ complexes. The molecular weight of each ERMES protein obtained after proteolytic treatment with thrombin (no histidine tag and/or MBP left) is indicated.

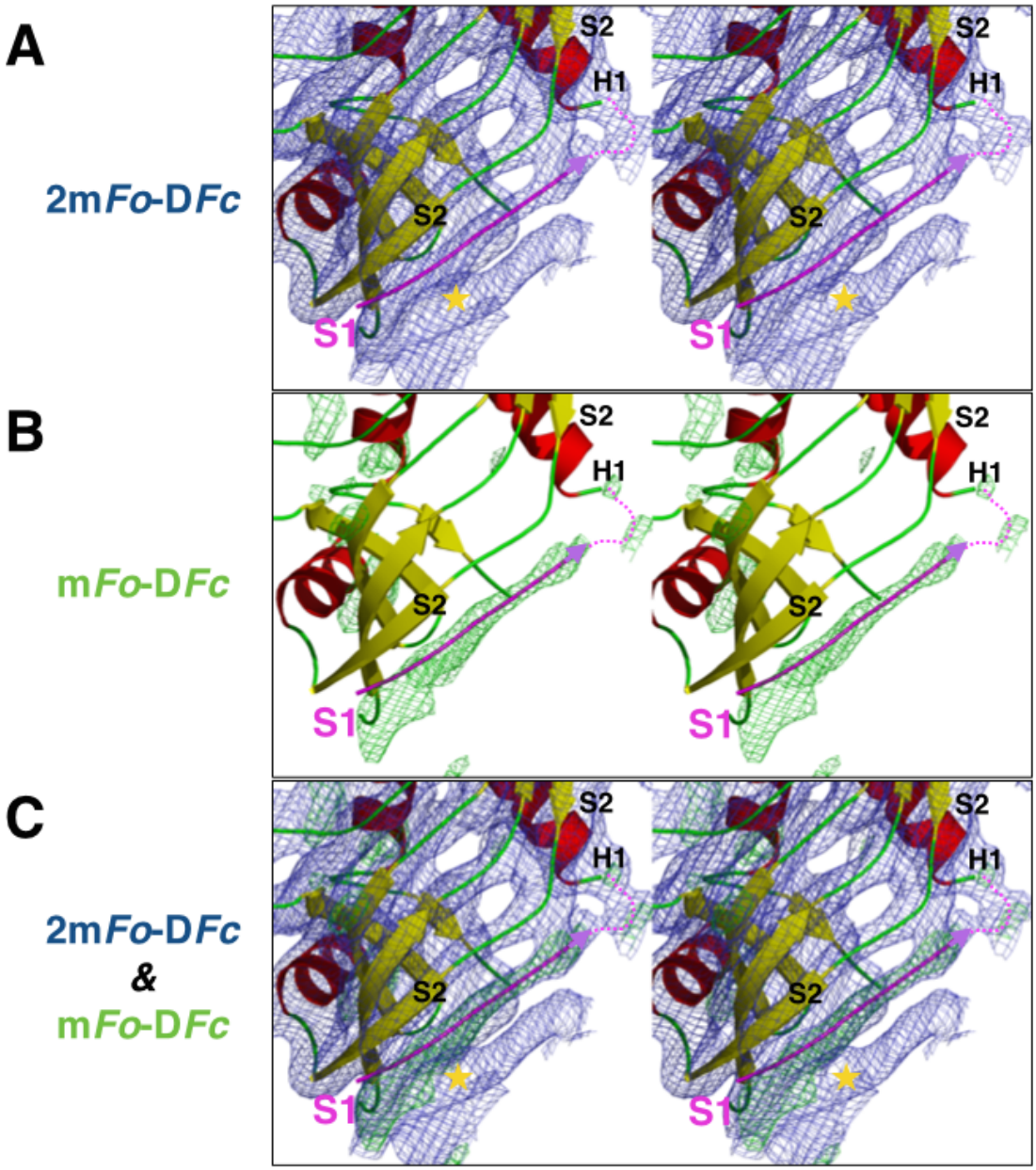

Fig. S2. **Unsharpened maximum likelihood weighted difference maps showing the non-swapped conformation of the N-terminal β-strand**. Stereo view of the initial 2m*Fo*-D*Fc* **(A)** and m*Fo*-D*Fc* **(B)** Fourier difference maps contoured at 1.1 σ and 3.0 σ, respectively, following molecular replacement in *Phaser* [7] and a single cycle of refinement in *Phenix* [8]. Molecular replacement was performed using the monomer of *Sce*-Mdm12 (PDB 5GYD) [5] as model where the 14 first N-terminal residues corresponding to the swapped β-strand S1 and the loop connecting with helix H1 were omitted. The backbone of Mdm12 is colored in red (helices), yellow (strands), and green (loops). The β-strand S1 drawn in magenta corresponds to the N-terminal β-strand S1 adopting a *non-swapped* conformation in our structure; it was *not* included in the initial model used for molecular replacement and the first cycle of refinement and is just shown to mark its true final position. (**C**) Same stereo view as in (**A**) and (**B**) but the two difference maps are shown superposed. These maps are *not* sharpened. The yellow star indicates a neighboring molecule (not displayed for clarity) related by crystallographic symmetry.

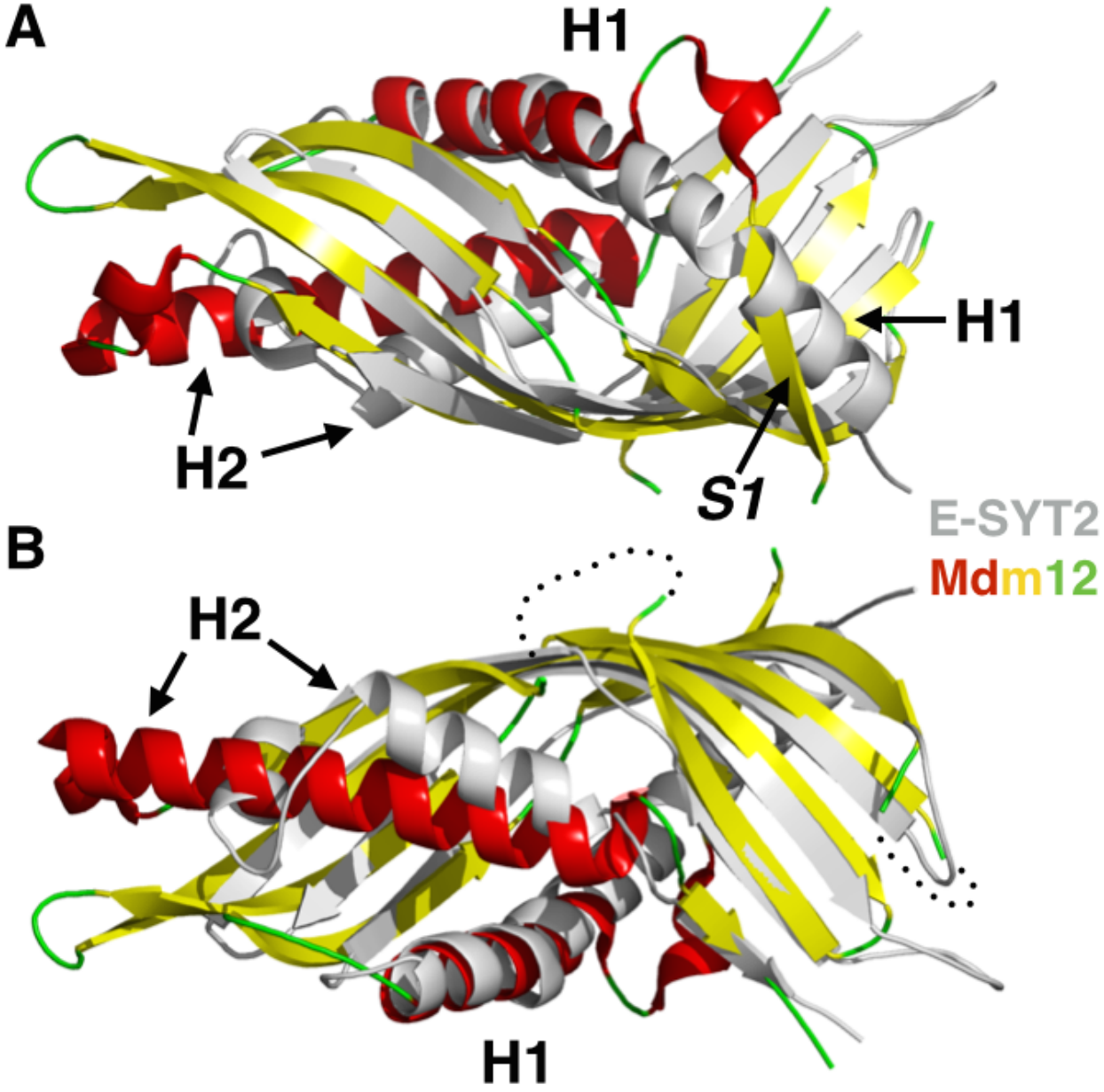

Fig. S3. **Superposition of the crystal structures of the SMP domains of Mdm12 and E-SYT2.** The superposed SMP folds observed in Mdm12 (yellow, green and red) and E-SYT2 (white) are shown in two different orientations (**A** and **B**) to highlight the most salient differences. For the sake of clarity, the two non-conserved insertions present in Mdm12 have been omitted and are shown as dotted lines. The two SMPs differ at their N-terminus with the presence of a N-terminal strand (S1) in Mdm12 replacing the bent N-terminus of the long α-helix H1 of E-SYT2. The other major difference is observed at the N-terminus of the α-helix H2; it is much shorter in the case of E-SYT2 [9]. The N-terminus of α-helix H1 of E-SYT2 is involved in its homo-dimerization, while the N-terminal β-strand S1 of Mdm12 that replaces it might play a similar role. In each SMP domain, the backbones of the antiparallel β-barrel formed by the 6 β-strands align remarkably well.

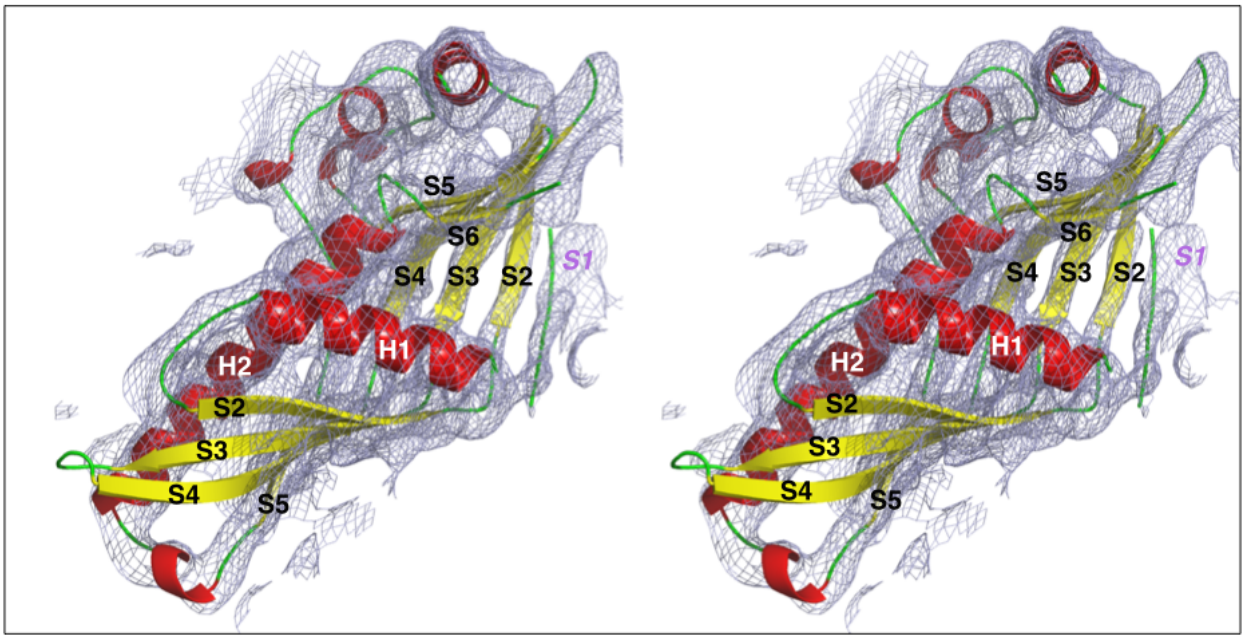

Fig. S4. Overall quality of the final maximum likelihood weighted 2m*Fo*-D*Fc* electron density for monomer A. Stereo-view of the unsharpened electron density map contoured at 1.3σ for the final refined structure shown in two different orientations. The non-swapped N-terminal β-strand S1 is highlighted in magenta. Secondary structure elements are labeled.

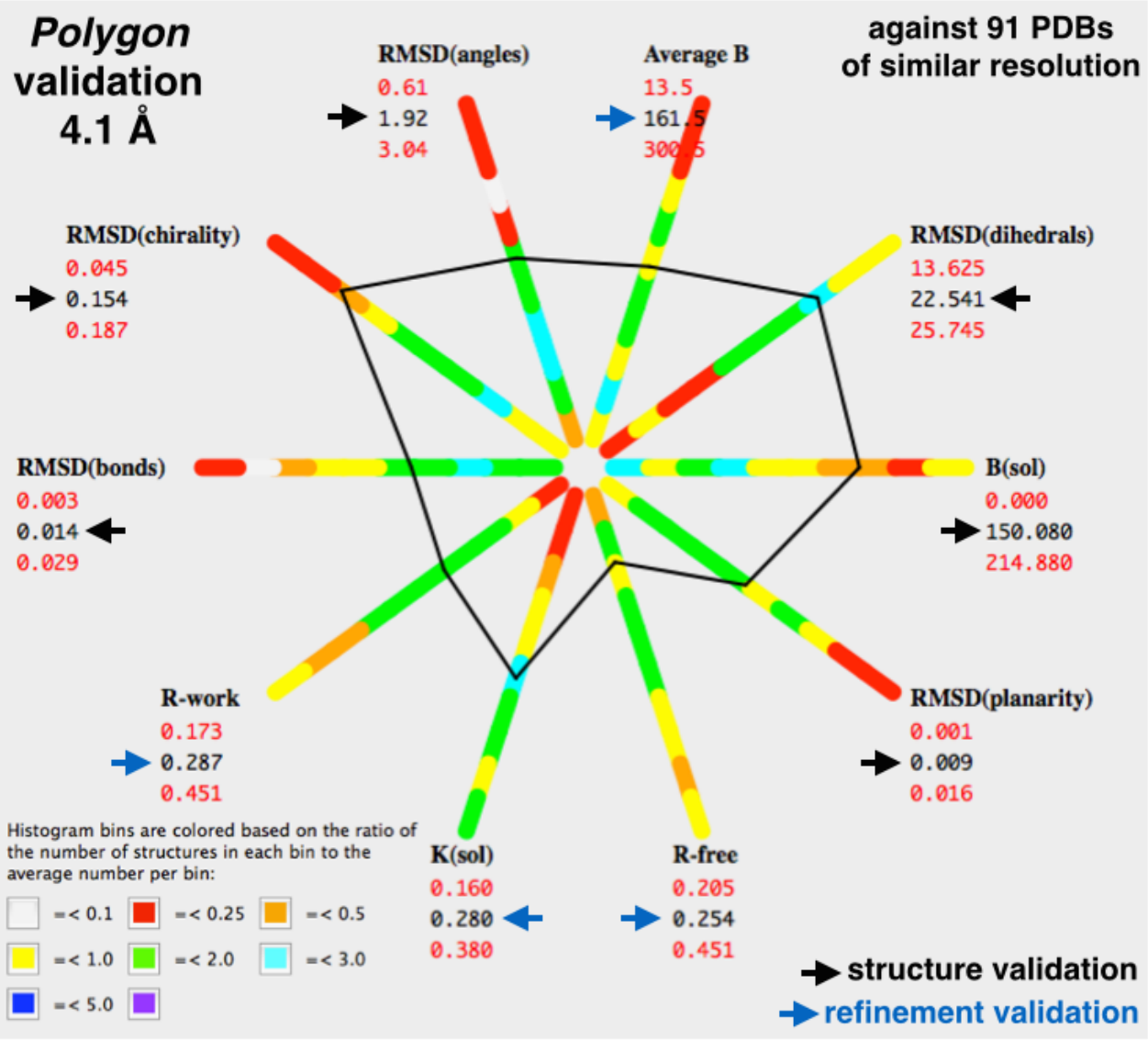

Fig. S5. **Structure and refinement quality assessment for the final model of *Sce*-Mdm12 refined at 4.1 Å resolution using *Polygon* analysis** [4]. The graph shows the histograms of the distribution across 91 PDB entries of similar resolution, with the range specified by numbers printed in red. Statistics for the current structure are printed in black (pointed by arrows); the connecting polygon (in black) shows where these values fall in the distribution.

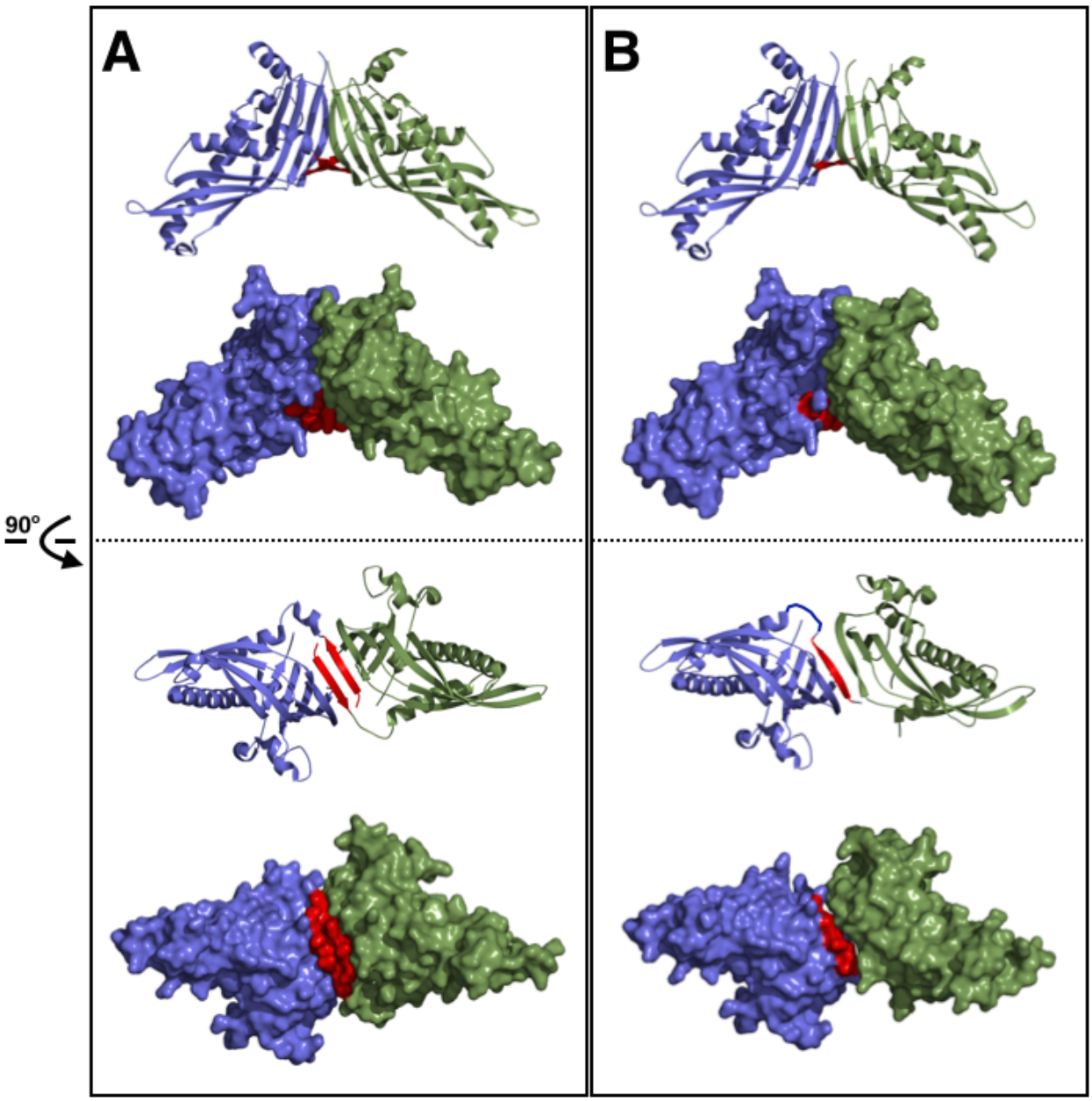

Fig. S6. The 'head-to-head' dimerization of the Mdm12 SMP/TULIP domain. Comparison between (**A**) the swapped 'head-to-head' dimer observed *in the asymmetric units* of structures 5GYD and 5GYK [5] and (**B**) our non-swapped 'head-to-head' pseudo-dimer observed *in the unit cell*. The N-terminal β-strand S1 is colored in red. Cartoon and surface representations are shown for two views (down the two-fold axis and perpendicular to the two-fold axis). Arrangement in (**A**) is the result of non-crystallographic symmetry while arrangement in (**B**) is a result of crystallographic symmetry.

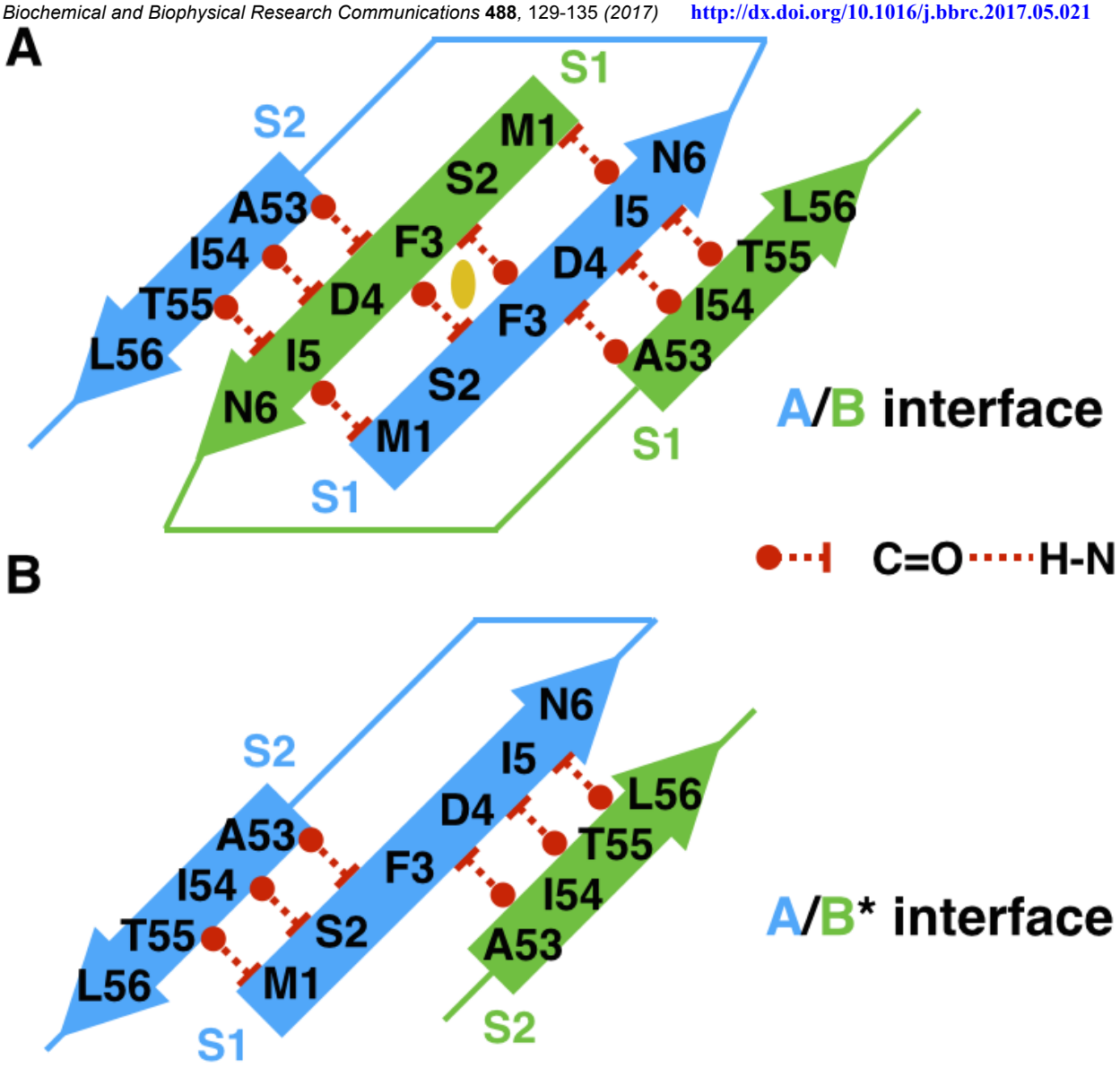

Fig. S7. Schematic of the interactions between the N-terminal β-strand S1 and the SMP/TULIP fold in Mdm12 (β-strand S2). (A) Swapping of N-terminal β-strands S1 at the two-fold symmetric 'head-to-head' dimerization interface described by Jeong *et al.* (PDBs 5GYD and 5GYK) [5]. **(B)** Asymmetric interface in the crystallographic 'head-to-head' pseudo-dimer interface observed in our structure.

References to Supplementary Data

[1] K. Diederichs, P.A. Karplus, Improved R-factors for diffraction data analysis in macromolecular crystallography, Nat Struct Biol 4 (1997) 269-275.
[2] P.A. Karplus, K. Diederichs, Linking crystallographic model and data quality, Science 336 (2012) 1030-1033.
[3] V.B. Chen, W.B. Arendall, 3rd, J.J. Headd, D.A. Keedy, R.M. Immormino, G.J. Kapral, L.W. Murray, J.S. Richardson, D.C. Richardson, MolProbity: all-atom structure validation for macromolecular crystallography, Acta Crystallogr D Biol Crystallogr 66 (2010) 12-21.
[4] L. Urzhumtseva, P.V. Afonine, P.D. Adams, A. Urzhumtsev, Crystallographic model quality at a glance, Acta Crystallographica Section D-Biological Crystallography 65 (2009) 297-300.
[5] H. Jeong, J. Park, C. Lee, Crystal structure of Mdm12 reveals the architecture and dynamic organization of the ERMES complex, EMBO Rep (2016).
[6] A.P. AhYoung, J. Jiang, J. Zhang, X. Khoi Dang, J.A. Loo, Z.H. Zhou, P.F. Egea, Conserved SMP domains of the ERMES complex bind phospholipids and mediate tether assembly, Proc Natl Acad Sci U S A 112 (2015) E3179-3188.
[7] A.J. McCoy, R.W. Grosse-Kunstleve, P.D. Adams, M.D. Winn, L.C. Storoni, R.J. Read, Phaser crystallographic software, J Appl Crystallogr 40 (2007) 658-674.
[8] P.D. Adams, P.V. Afonine, G. Bunkoczi, V.B. Chen, N. Echols, J.J. Headd, L.W. Hung, S. Jain, G.J. Kapral, R.W. Grosse Kunstleve, A.J. McCoy, N.W. Moriarty, R.D. Oeffner, R.J. Read, D.C. Richardson, J.S. Richardson, T.C. Terwilliger, P.H. Zwart, The Phenix software for automated determination of macromolecular structures, Methods 55 (2011) 94-106.
[9] C.M. Schauder, X. Wu, Y. Saheki, P. Narayanaswamy, F. Torta, M.R. Wenk, P. De Camilli, K.M. Reinisch, Structure of a lipid-bound extended synaptotagmin indicates a role in lipid transfer, Nature (2014).